Frontiers in Bioscience Landmark

Front. Biosci. (Landmark Ed) **2026**; 31(9): 55382
https://doi.org/10.31083/FBL55382

Original Research

TGM2 Activates the ERK Signaling Pathway to Disrupt Intestinal Barrier Function and Aggravate Colitis

Hong Dai[1,2,†], Longfei Dai[3,†], Yufeng Xu[1], Xiaojing Liu[2,*]

[1]Department of Pediatrics, Huaibei People's Hospital, 235025 Huaibei, Anhui, China
[2]Department of Pediatrics, The First Affiliated Hospital of Anhui Medical University, 230022 Hefei, Anhui, China
[3]Department of General Surgery, The First Affiliated Hospital of Anhui Medical University, 230022 Hefei, Anhui, China
*Correspondence: hudie107@163.com (Xiaojing Liu)
[†]These authors contributed equally.

Academic Editor: Xiaolei Tang
Submitted: 28 June 2026 Revised: 6 August 2026 Accepted: 14 August 2026 Published: 15 September 2026

Abstract

Background: PANoptosis-related transcriptional programs may contribute to pediatric ulcerative colitis (UC), but the genes most consistently associated with disease activity and epithelial injury remain uncertain. **Methods:** Public transcriptomic cohorts were integrated with machine-learning feature selection, treatment-response analyses, immune cell deconvolution, molecular clustering, and two-sample Mendelian randomization (MR). Transglutaminase 2 (TGM2) expression was examined in colonic specimens from six pediatric patients with UC and six controls. TGM2 knockdown was evaluated in lipopolysaccharide-stimulated HT29 cells using inflammatory gene analysis, tight junction protein measurements, RNA sequencing, and MAPK signaling assays. **Results:** A total of 17 differentially expressed PANoptosis-related genes were identified, and *CCL2*, *JAK3*, and *TGM2* were prioritized as candidate genes. In the external GSE126124 cohort, *TGM2* yielded an area under the curve of 0.918 in colonic tissue and 0.744 in peripheral blood. *TGM2* expression was associated with disease activity, inflammatory cell estimates, barrier-related gene expression, and treatment response. Six single-nucleotide polymorphisms (SNPs) were included in the MR analysis. The inverse-variance weighted estimate was significant (odds ratio 1.486, 95% confidence interval 1.055–2.092; $p = 0.023$), whereas the other four methods were not significant. In LPS-stimulated HT29 cells, TGM2 knockdown was accompanied by lower *TNF-α*, *IL-1β*, and *IL-6* expression, increased ZO-1, Occludin, and Claudin-3 abundance, and reduced ERK phosphorylation; substantial changes in JNK or p38 phosphorylation were not detected. **Conclusion:** TGM2 was identified as a candidate through PANoptosis-related bioinformatic screening. TGM2 expression was associated with pediatric UC activity and treatment response, whereas TGM2 knockdown was associated with reduced inflammatory gene expression, increased tight junction protein abundance, and lower ERK phosphorylation in LPS-stimulated HT29 cells. Functional involvement of TGM2 in PANoptosis and its mechanistic position within ERK signaling require further validation.

Keywords: ulcerative colitis; child; regulated cell death; protein glutamine gamma glutamyltransferase 2; mendelian randomization analysis

1. Introduction

Ulcerative colitis (UC) is a chronic inflammatory bowel disease characterized by persistent inflammation of the colonic mucosa [1]. Although UC most commonly manifests in young adults, approximately 10% of cases occur in pediatric patients, and both the incidence and prevalence of pediatric UC have been increasing worldwide [2]. Once predominantly confined to developed regions, pediatric UC has shown a marked rise in developing countries in recent years, underscoring its growing global health burden [3,4].

The pathogenesis of UC is multifactorial and involves complex interactions among metabolic alterations, epithelial barrier dysfunction, microbial dysbiosis, and immune dysregulation [5]. Reduced production of short-chain fatty acids, impaired synthesis of mucin-2, and decreased microbial diversity collectively compromise the integrity of the intestinal barrier. Disruption of this barrier permits inappropriate interactions between luminal microbes and the mucosal immune system, resulting in sustained and dysregulated inflammatory responses within the colonic mucosa [6]. In pediatric patients, UC poses additional challenges beyond intestinal inflammation, including impaired linear growth, delayed pubertal development, and long-term psychological and physical consequences during critical developmental stages [7]. Notably, even during clinical remission, a substantial proportion of pediatric patients continue to experience persistent symptoms such as abdominal pain and fatigue, reflecting a heightened vulnerability in this population.

Current therapeutic strategies for pediatric UC rely primarily on pharmacological interventions, including aminosalicylates such as mesalazine [8], corticosteroids, immunomodulators, and biologic agents targeting key inflammatory pathways, including infliximab (IFX) and vedolizumab (VDZ) [9,10,11]. These treatments aim to

induce and maintain remission, promote mucosal healing, and improve quality of life. However, considerable limitations remain, including heterogeneous treatment responses, treatment-related adverse effects, and a lack of long-term, pediatric-specific safety and efficacy data. In refractory disease, surgical intervention may be required, further highlighting the unmet need for improved mechanistic understanding and targeted therapeutic approaches in pediatric UC.

PANoptosis is a recently defined inflammatory form of programmed cell death that integrates components of pyroptosis, apoptosis, and necroptosis into a unified molecular framework [12,13]. As an innate immune–driven cell death pathway, PANoptosis has been increasingly implicated in the pathogenesis of inflammatory diseases, where its dysregulation can promote excessive inflammation, epithelial barrier disruption, and aberrant immune activation [14,15]. Experimental studies have demonstrated that ZBP1-mediated PANoptosis plays a critical role in interferon-driven inflammatory responses, and genetic ablation of ZBP1 has been shown to attenuate severe intestinal inflammation in mice with intestinal epithelial cell–specific deletion of SETDB1 [16,17]. These observations suggest that PANoptosis may represent a central regulatory node linking epithelial injury to mucosal inflammation in the intestine.

Despite accumulating evidence implicating regulated cell-death programs in intestinal inflammation, the genes associated with PANoptosis-related transcriptional changes in pediatric UC remain poorly defined. Identification of such genes may support disease stratification and generate testable mechanistic hypotheses. In this study, transglutaminase 2 (TGM2) was prioritized as a PANoptosis-related candidate through integrative bioinformatic screening. Its associations with disease activity, treatment response, inflammatory features, epithelial junctional proteins, and MAPK signaling were subsequently examined. This design was intended to nominate TGM2 for further investigation rather than to establish it as a functional regulator of PANoptosis or a direct therapeutic target.

2. Methods

2.1 Data Acquisition and Preprocessing

Four publicly available pediatric UC transcriptomic datasets (GSE107499, GSE109142, GSE87473, and GSE126124) were retrieved from the Gene Expression Omnibus (GEO) database. The GSE126124 cohort comprised both intestinal tissue and peripheral blood samples, whereas the remaining datasets consisted exclusively of colonic tissue samples. Raw expression data were converted into standardized gene expression matrices based on the corresponding platform annotation files. After preprocessing, GSE107499, GSE109142, and GSE87473 were merged into a single integrated cohort (Merge-cohort). This merged dataset was randomly divided into a training set and an internal validation set at a ratio of 7:3. The GSE126124 cohort was retained as an independent external validation dataset.

2.2 Identifying PANoptosis-Related Differential Genes

Differentially expressed genes (DEGs) between pediatric UC samples and non-inflamed controls in the training set were identified using a threshold of $|\log_2$ fold change$|$ >1.5 and a nominal p value < 0.05. A curated list of PANoptosis-related genes (PRGs) was compiled from previously published studies (**Supplementary Table 1**). Overlapping genes between the DEGs and PRGs were defined as PANoptosis-related DEGs involved in pediatric UC. Functional interaction networks and pathway enrichment analyses of these genes were performed using GeneMANIA [18] and Metascape [19] to identify significantly enriched biological processes and signaling pathways.

2.3 Machine Learning–Based Identification of Key PANoptosis Genes

To identify critical PANoptosis-associated genes, twelve machine learning algorithms were implemented, including LASSO, Ridge regression, Elastic Net, stepwise generalized linear modeling (Stepglm), support vector machine (SVM), glmBoost, linear discriminant analysis (LDA), partial least squares regression for generalized linear models (plsRglm), random forest (RF), gradient boosting machine (GBM), extreme gradient boosting (XGBoost), and Naïve Bayes, resulting in a total of 113 machine-learning algorithm combinations. Genes consistently selected across multiple algorithms were defined as key PANoptosis genes. The diagnostic performance of these genes in distinguishing pediatric UC from controls was evaluated using receiver operating characteristic (ROC) curve analysis, and the area under the curve (AUC) was used for comparative assessment.

2.4 Evaluation of Key Gene Expression in Drug-Treated UC Cohorts

Three additional GEO datasets (GSE16879, GSE73661, and GSE92415) were analyzed to examine treatment-associated changes in candidate-gene expression. Expression was compared before and after infliximab, vedolizumab, or golimumab treatment and between responders and non-responders. Associations between candidate-gene expression and disease activity were evaluated using the Mayo score [20], with higher scores indicating more severe disease activity.

2.5 Immune Infiltration Analysis and Correlation With PANoptosis Genes

Immune cell infiltration was estimated using five complementary computational algorithms: single-sample gene set enrichment analysis (ssGSEA), CIBERSORT [21], MCP-counter, xCell [22], and EPIC [23]. These approaches

were applied to quantify the relative abundance of immune cell subsets in UC samples. Spearman correlation analysis was subsequently conducted to assess relationships between key PANoptosis genes and immune cell populations. Correlations between key genes, pro-inflammatory cytokines, and intestinal barrier–associated proteins were also systematically evaluated.

2.6 Consensus Clustering Analysis

Unsupervised consensus clustering was performed to stratify pediatric UC patients into molecular subgroups based on the expression profiles of the candidate genes. Differences among clusters were analyzed with respect to inflammatory-gene expression, intestinal barrier-related genes, and estimated immune-cell infiltration. Gene set enrichment analysis (GSEA) was applied to identify biological pathways preferentially enriched in each cluster using the established GSEA framework.

2.7 Mendelian Randomization Analysis

Two-sample MR was conducted to explore the association between genetically predicted TGM2 expression and UC risk. Expression quantitative trait-locus data were obtained from large-scale genome-wide association studies [24], and UC outcome data were retrieved from the FinnGen consortium. Six harmonized SNPs were included in the final analysis (rs7955767, rs17787900, rs225245, rs12624511, rs8887, and rs1666873). Five methods implemented in the TwoSampleMR package were applied: inverse-variance weighted (IVW), MR-Egger, weighted median, simple mode, and weighted mode. MR-PRESSO was used to screen for outliers, heterogeneity was assessed with IVW and MR-Egger tests, horizontal pleiotropy was evaluated with the MR-Egger intercept, and leave-one-out analysis was used to examine the influence of individual SNPs.

2.8 Molecular Docking and Experimental Validation

Molecular docking analysis was performed to predict the binding affinity and interaction modes between mesalazine and candidate target proteins. The three-dimensional structure of mesalazine was retrieved from the PubChem database, and protein structures were obtained from the Protein Data Bank (PDB). Ligand energy minimization was conducted using the MM2 force field, followed by docking simulations performed with AutoDock Vina. Docking conformations and interaction patterns were visualized using PyMOL.

For clinical validation, colonic mucosal biopsies were obtained from pediatric patients diagnosed with ulcerative colitis (UC) and age-matched healthy controls at Huaibei People's Hospital. UC was diagnosed according to the revised Porto criteria by integrating clinical presentation, endoscopic findings, histopathological evaluation, and laboratory results. Control tissues were collected from individuals who underwent colonoscopy for colorectal screening or functional gastrointestinal symptoms and showed no evidence of intestinal inflammation or other organic bowel diseases. Patients with autoimmune disorders, infectious colitis, malignancies, or a history of intestinal surgery were not included. After collection, tissue specimens were immediately frozen in liquid nitrogen and stored at −80 °C until further analysis. The study was approved by the Ethics Committee of Huaibei People's Hospital (No. 2023-109), and written informed consent was obtained from all participants or their legal guardians prior to sample collection.

Human colorectal epithelial HT29 cells (catalog no. SCSP-5032) were purchased from the Cell Bank of the Chinese Academy of Sciences (Shanghai, China). The cell lines were validated by STR profiling and tested negative for mycoplasma. Cells were maintained in DMEM (Gibco, USA) supplemented with 10% fetal bovine serum, 100 U/mL penicillin, and 100 μg/mL streptomycin under standard culture conditions (37 °C, 5% CO_2). The culture medium was refreshed every 2–3 days, and cells in the exponential growth phase were used for all experiments.

Stable TGM2-silenced HT29 cells were generated by lentiviral infection with shRNA targeting human TGM2 (GenePharma, Shanghai, China). Polybrene (8 μg/mL) was added during transduction to improve infection efficiency, followed by puromycin selection (2 μg/mL) for 7–10 days to establish stable cell lines. Knockdown efficiency was confirmed by quantitative real-time PCR (qRT-PCR) together with Western blot analysis. The primer sequences employed in this study were designed and supplied by Sangon Biotech Co., Ltd. (Shanghai, China), and are presented in **Supplementary Table 2**. Cells infected with a scrambled shRNA vector served as the negative control.

The following primary antibodies were used: GAPDH (Cat. No. 60004-1-Ig; Proteintech, Wuhan, Hubei, China), TGM2 (Cat. No. 15100-1-AP; Proteintech, Wuhan, Hubei, China), Occludin (Cat. No. 27260-1-AP; Proteintech, Wuhan, Hubei, China), Claudin 3 (Cat. No. 86697-1-RR; Proteintech, Wuhan, Hubei, China), ZO-1 (Cat. No. 21773-1-AP; Proteintech, Wuhan, Hubei, China), p38 (Cat. No. 14064-1-AP; Proteintech, Wuhan, Hubei, China), Phospho-p38 (Cat. No. 28796-1-AP; Proteintech, Wuhan, Hubei, China), JNK (Cat. No. 51153-1-AP; Proteintech, Wuhan, Hubei, China), Phospho-JNK (Cat. No. 80024-1-RR; Proteintech, Wuhan, Hubei, China), ERK1/2 (Cat. No. 11257-1-AP; Proteintech, Wuhan, Hubei, China), and Phospho-ERK1/2 (Cat. No. 80031-1-RR; Proteintech, Wuhan, Hubei, China).

To mimic an inflammatory environment, HT29 cells were exposed to lipopolysaccharide (LPS, Escherichia coli O111; Sigma-Aldrich, USA) at a concentration of 1 μg/mL for 24 h, while untreated cells were used as controls. Total RNA was extracted with TRIzol reagent (Invitrogen, USA) following the manufacturer's protocol. RNA quality was assessed using a NanoDrop 2000 spectrophotometer and an

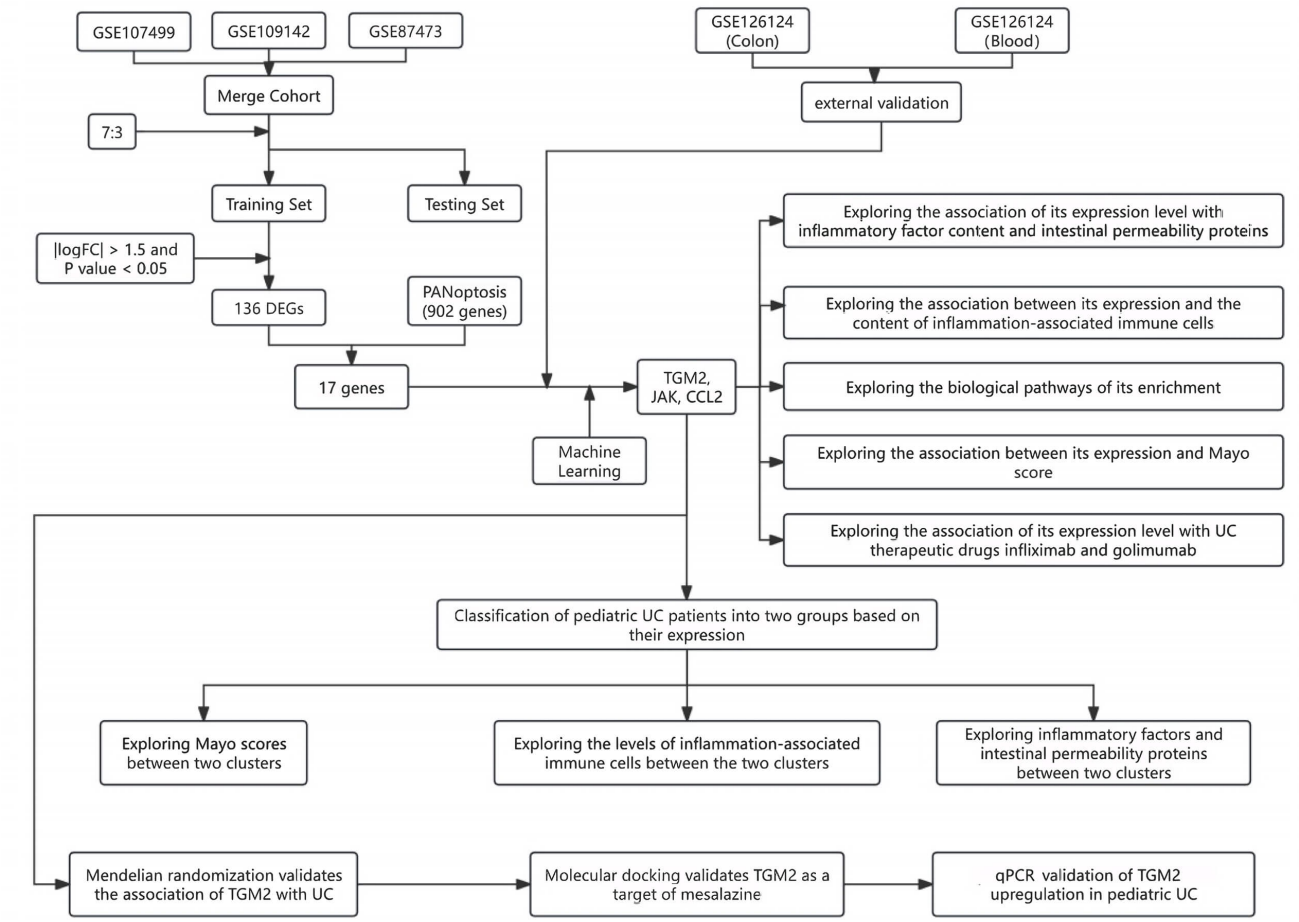

Fig. 1. Overall study design. Public pediatric UC transcriptomic cohorts were integrated for differential-expression analysis and PANoptosis-related gene screening. Candidate genes were prioritized by machine-learning algorithms and evaluated in diagnostic, treatment, immune-infiltration, clustering, and MR analyses. TGM2 was then examined in pediatric colonic specimens and LPS-stimulated HT29 cells, followed by transcriptomic, MAPK-signaling, and molecular-docking analyses. UC, ulcerative colitis; MR, Mendelian randomization; TGM2, transglutaminase 2; LPS, lipopolysaccharide; MAPK, mitogen-activated protein kinase.

Agilent 2100 Bioanalyzer, and only samples with an RNA integrity number (RIN) of at least 7.0 were included for sequencing.

RNA libraries were prepared using the NEBNext Ultra RNA Library Prep Kit (New England Biolabs, USA) and sequenced on the Illumina NovaSeq 6000 platform by Novogene (Beijing, China). Following removal of adaptor sequences and low-quality reads, the clean reads were aligned to the human reference genome (GRCh38). Gene expression levels were calculated as fragments per kilobase of transcript per million mapped reads (FPKM). Differential expression analysis was carried out using the DESeq2 package, with $|\log_2$ fold change$| \geq 1.0$ and adjusted $p \leq 0.05$ defined as the significance thresholds. Gene Ontology (GO) and Kyoto Encyclopedia of Genes and Genomes (KEGG) enrichment analyses were subsequently performed to explore biological functions and signaling pathways associated with TGM2 under inflammatory conditions.

2.9 Statistical Analysis

All computational analyses were performed using R software (version 4.3.2; R Core Team, Vienna, Austria) and Strawberry Perl (open-source; https://strawberryperl.com), and experimental data were analyzed using GraphPad Prism (version 9.0; GraphPad Software, San Diego, CA, USA). Before parametric or non-parametric tests were selected, the distribution of continuous data within each comparison group was assessed using the Shapiro–Wilk test, and homogeneity of variance was evaluated before parametric testing. Normally distributed data are presented as the mean ± standard deviation, whereas non-normally distributed data are presented as the median with interquartile range. Two independent groups were compared using an unpaired two-tailed Student's *t*-test when the assumptions of normality and equal variance were satisfied; otherwise, the Mann–Whitney U test was applied. For comparisons involving more than two groups, one-way analysis of variance followed by Tukey's multiple-comparisons test was used for

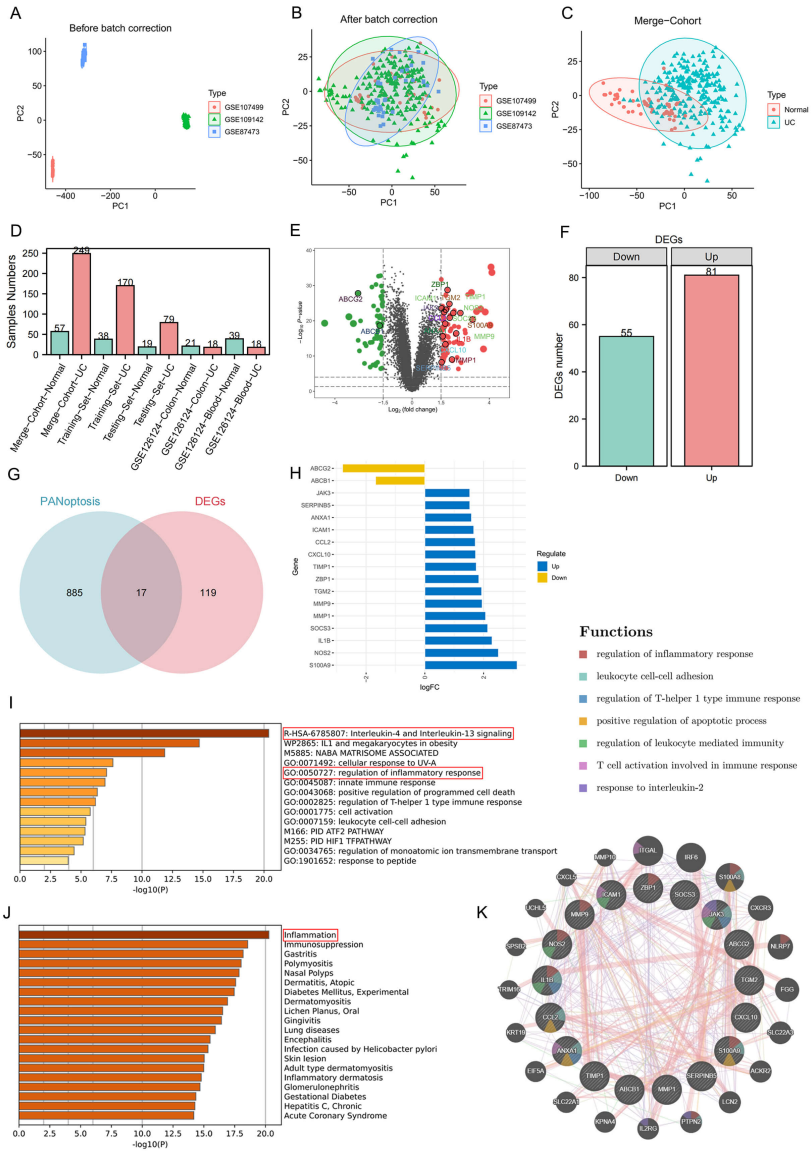

Fig. 2. Identification and characterization of 17 PANoptosis-related differentially expressed genes in pediatric ulcerative colitis. (A) Principal component analysis (PCA) of GSE107499, GSE109142, and GSE87473 before batch-effect correction, in which clear separation among the three datasets was observed. (B) PCA after batch-effect correction, in which improved integration of samples from the three datasets was demonstrated. (C) PCA of the merged cohort, in which control and pediatric UC samples were separated according to their expression profiles. (D) Numbers of control and pediatric UC samples included in the merged cohort, training set, testing set, GSE126124 colonic tissue cohort, and GSE126124 peripheral blood cohort. (E) Volcano plot of differentially expressed genes (DEGs) between control and pediatric UC samples in the merged cohort. Upregulated and downregulated genes are shown in red and green, respectively. (F) Numbers of upregulated and downregulated DEGs; 81 genes were upregulated and 55 genes were downregulated. (G) Venn diagram showing the intersection between 136 DEGs and 902 PANoptosis-related genes, from which 17 overlapping genes were identified. (H) Expression changes of the 17 PANoptosis-related DEGs; 15 genes were upregulated and 2 genes were downregulated in pediatric UC. (I) Functional enrichment analysis of the 17 overlapping genes, in which inflammation- and immune-related biological processes were identified. The red box was used to highlight the significantly enriched pathways associated with the 17 differentially expressed genes, particularly inflammation-related pathways, including IL-4 and IL-13 signaling and inflammatory response pathways. (J) Disease enrichment analysis showing the diseases associated with the 17 overlapping genes. The red box was used to highlight the results of DisGeNET disease enrichment analysis, showing that these 17 differentially expressed genes were significantly enriched in inflammation-related diseases, with inflammatory disease ranking as the top enriched disease category. (K) Protein-protein interaction network of the 17 PANoptosis-related DEGs and their functionally associated proteins.

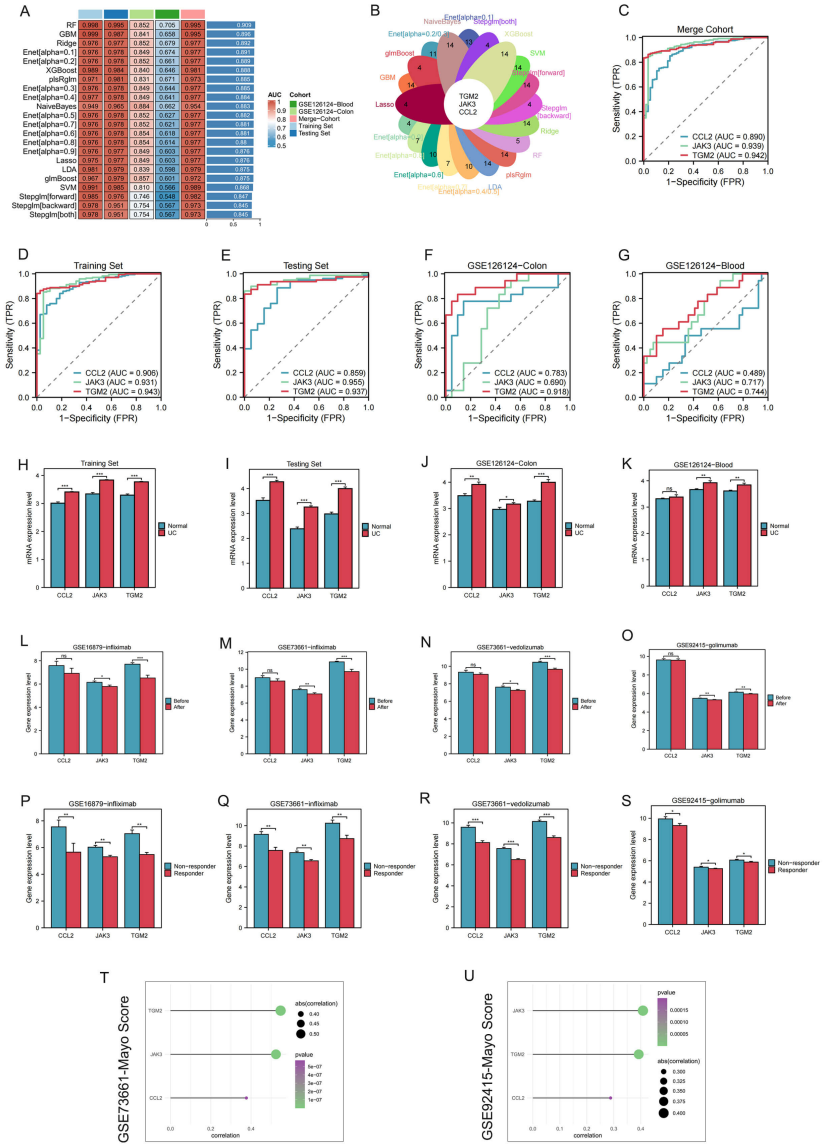

Fig. 3. Identification and clinical relevance of PANoptosis-associated candidate genes in pediatric ulcerative colitis. (A) Predictive models generated using 12 machine-learning algorithms were evaluated in the training set, testing set, merged cohort, GSE126124 colonic tissue cohort, and GSE126124 peripheral blood cohort. The random forest model achieved the highest overall C-index. (B) Genes selected by the 12 machine-learning algorithms were compared, and *CCL2*, *JAK3*, and *TGM2* were identified as shared candidate genes. (C) Receiver operating characteristic (ROC) curves for *CCL2*, *JAK3*, and *TGM2* in the merged cohort, with AUC values of 0.890, 0.939, and 0.942, respectively. (D) ROC curves in the training set, with AUC values of 0.906, 0.931, and 0.943 for *CCL2*, *JAK3*, and *TGM2*, respectively. (E) ROC curves in the testing set, with AUC values of 0.859, 0.955, and 0.937 for *CCL2*, *JAK3*, and *TGM2*, respectively. (F) ROC curves in the GSE126124 colonic tissue cohort, with AUC values of 0.783, 0.690, and 0.918 for *CCL2*, *JAK3*, and *TGM2*, respectively. (G) ROC curves in the GSE126124 peripheral blood cohort, with AUC values of 0.489, 0.717, and 0.744 for *CCL2*, *JAK3*, and *TGM2*, respectively. (H–K) Expression levels of *CCL2*, *JAK3*, and *TGM2* in control and pediatric UC samples from the training set, testing set, GSE126124 colonic tissue cohort, and GSE126124 peripheral blood cohort, respectively. (L) Expression levels of the three genes before and after infliximab treatment in GSE16879. (M) Expression levels before and after infliximab treatment in GSE73661. (N) Expression levels before and after vedolizumab treatment in GSE73661. (O) Expression levels before and after golimumab treatment in GSE92415. (P) Expression levels of the three genes in infliximab responders and non-responders from GSE16879. (Q) Expression levels in infliximab responders and non-responders from GSE73661. (R) Expression levels in vedolizumab responders and non-responders from GSE73661. (S) Expression levels in golimumab responders and non-responders from GSE92415. (T) Correlations between *CCL2*, *JAK3*, and *TGM2* expression and Mayo scores in GSE73661. (U) Correlations between the expression of the three genes and Mayo scores in GSE92415. $^{*}p < 0.05$, $^{**}p < 0.01$, and $^{***}p < 0.001$; ns, not significant.

normally distributed data, whereas the Kruskal–Wallis test followed by Dunn's multiple-comparisons test was used for non-normally distributed data. All tests were two-sided, and $p < 0.05$ was considered statistically significant.

3. Results

The design flowchart of this study is presented in Fig. 1.

3.1 Seventeen PANoptosis-Related Genes are Differentially Expressed in Pediatric UC

After batch-effect correction, samples from the three pediatric UC cohorts exhibited satisfactory integration, as demonstrated by principal component analysis (Fig. 2A,B). Clear separation between control and pediatric UC samples was observed in the merged cohort (Fig. 2C). The merged dataset was randomly divided into a training set and an internal validation set at a ratio of 7:3 (Fig. 2D). Differential expression analysis identified 136 genes that were significantly dysregulated in pediatric UC, including 81 upregulated and 55 downregulated genes (Fig. 2E,F). Intersection with curated PANoptosis-related genes yielded 17 PANoptosis-associated differentially expressed genes (PRGs) (Fig. 2G). Except for *ABCG2* and *ABCB1*, which were downregulated, the remaining 15 PRGs were significantly upregulated in pediatric UC (Fig. 2H). Protein–protein interaction (PPI) analysis using the GeneMANIA database revealed extensive interactions among proteins encoded by these PRGs (Fig. 2K). Functional enrichment analysis demonstrated that these genes were predominantly involved in inflammation-related pathways, particularly interleukin signaling pathways such as IL4, IL13, and IL1 signaling (Fig. 2I), and were significantly associated with inflammatory disease processes (Fig. 2J).

3.2 CCL2, JAK3, and TGM2 are PANoptosis-Related Candidate Genes With Diagnostic and Treatment-Associated Expression Patterns in Pediatric UC

113 machine-learning algorithms were applied to prioritize the 17 PANoptosis-related differentially expressed genes and construct predictive models for pediatric UC. The random forest model showed the highest overall performance, with a C-index of 0.909 in both the training and validation cohorts (Fig. 3A). Cross-comparison of the selected features identified *CCL2*, *JAK3*, and *TGM2* as shared candidate genes (Fig. 3B). In the merged cohort, the AUC values were 0.890 for CCL2, 0.939 for *JAK3*, and 0.942 for *TGM2*. The corresponding values were 0.906, 0.931, and 0.943 in the training set and 0.859, 0.955, and 0.937 in the testing set. In GSE126124, the tissue AUC values were 0.783, 0.690, and 0.918, and the peripheral-blood AUC values were 0.489, 0.717, and 0.744, respectively (Fig. 3C–G). All three genes were upregulated in pediatric UC samples (Fig. 3H–K). JAK3 and TGM2 expression was lower after infliximab, vedolizumab, or golimumab treatment, and lower expression of the three genes was observed in responders than in non-responders in the indicated cohorts (Fig. 3L–S). These treatment-associated differences may reflect attenuation of inflammatory activity and do not demonstrate direct drug targeting. Expression of the three genes was positively correlated with Mayo scores (Fig. 3T,U).

3.3 Expression of CCL2, JAK3, and TGM2 Is Associated With Inflammatory Infiltration and Intestinal Barrier-Related Transcriptional Changes

Gene set enrichment analyses (GSEA) associated higher *CCL2*, *JAK3*, and *TGM2* expression with inflammation-related pathways, including MAPK, Toll-like receptor, and JAK-STAT signaling (Fig. 4A–C). Five complementary deconvolution algorithms estimated differences in immune-cell composition between control and pediatric UC samples (Fig. 4D and **Supplementary Fig. 1**). *CCL2*, *JAK3*, and *TGM2* expression were positively correlated with several pro-inflammatory cell estimates and negatively correlated with M2 macrophage estimates (Fig. 4E,F). The three genes were also positively correlated with inflammatory mediators, including *COX2*, *ICAM1*, *IFNG*, *IL1A*, *IL1B*, *NFKB1*, *NLRP3*, *TLR4*, and *TNF* (Fig. 4G). Conversely, their expression was inversely correlated with Claudin-3, Occludin, ZO-1, and E-cadherin and positively correlated with N-cadherin (Fig. 4H). These findings suggest that the expression levels of *CCL2*, *JAK3*, and *TGM2* are associated with intestinal inflammation and intestinal permeability.

3.4 Pediatric UC Patients Can Be Stratified Into Molecular Subtypes With Distinct Disease Severity

Consensus clustering based on the expression of *CCL2*, *JAK3*, and *TGM2* stratified pediatric UC patients into two distinct molecular clusters (Fig. 5A), which were clearly separated by principal component analysis (Fig. 5B). Cluster 1 exhibited significantly higher expression of all three genes (Fig. 5C) and was associated with elevated Mayo scores, indicating more severe disease activity (Fig. 5D,E). Cluster 1 also displayed increased expression of multiple pro-inflammatory genes (Fig. 5G) and reduced expression of intestinal barrier–related genes (*OCLN*, *CLDN3*, and *E-cadherin*) (Fig. 5F). Pathway enrichment analysis revealed significant activation of inflammation-related pathways in Cluster 1, including MAPK signaling, chemokine signaling, and Toll-like receptor signaling (Fig. 5H). Immune infiltration analysis further demonstrated increased abundance of pro-inflammatory immune cells in Cluster 1, whereas Cluster 2 was characterized by higher levels of M2 macrophages (Fig. 5I, **Supplementary Fig. 2**).

Two-sample MR was used to explore the association between genetically predicted TGM2 expression and UC risk. Six instrumental SNPs were included. The IVW method indicated an association with UC risk (OR 1.486,

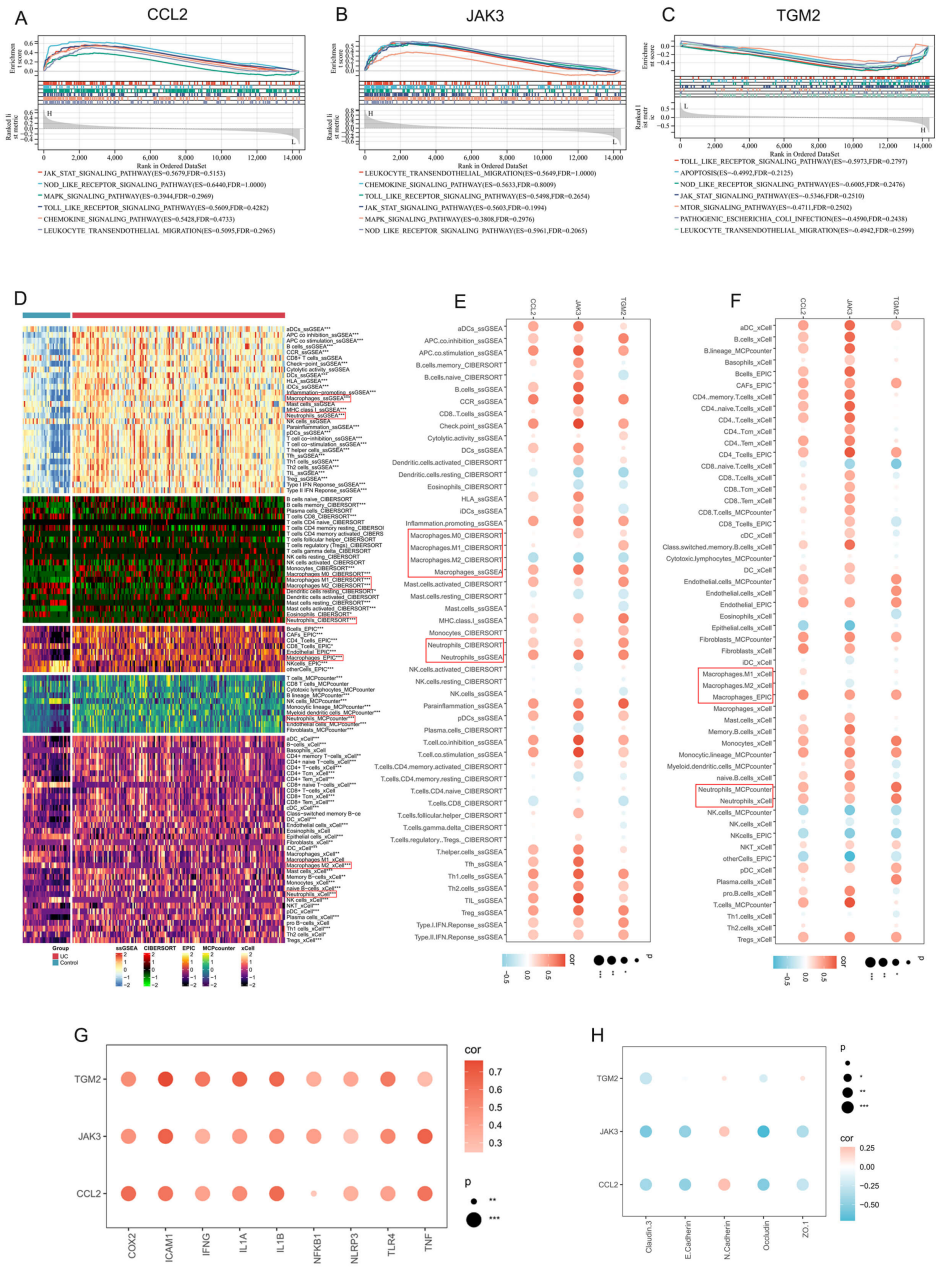

Fig. 4. Associations of *CCL2*, *JAK3*, and *TGM2* with inflammatory pathways, immune-cell infiltration, and intestinal barrier-related genes in pediatric ulcerative colitis. (A) GSEA showing signaling pathways associated with *CCL2* expression, including the JAK–STAT, NOD-like receptor, MAPK, Toll-like receptor, chemokine, and leukocyte transendothelial migration pathways. (B) GSEA showing immune- and inflammation-related pathways associated with *JAK3* expression. (C) GSEA showing signaling pathways associated with *TGM2* expression, including the Toll-like receptor, apoptosis, NOD-like receptor, JAK–STAT, pathogenic Escherichia coli infection, and leukocyte transendothelial migration pathways. (D) Heatmap showing differences in the estimated abundance of immune-cell populations between control and pediatric ulcerative colitis (UC) samples. Immune-cell abundance was estimated using ssGSEA, CIBERSORT, EPIC, MCP-counter, and xCell. (E,F) Correlations of *CCL2*, *JAK3*, and *TGM2* expression with immune-cell populations estimated using the five algorithms. Positive and negative correlations are shown in red and blue, respectively. (G) Correlations of *CCL2*, *JAK3*, and *TGM2* expression with the inflammatory genes *COX2*, *ICAM1*, *IFNG*, *IL1A*, *IL1B*, *NFKB1*, *NLRP3*, *TLR4*, and *TNF*. (H) Correlations of *CCL2*, *JAK3*, and *TGM2* expression with the intestinal barrier-related genes Claudin-3, E-cadherin, N-cadherin, Occludin, and ZO-1. Dot color represents the direction and strength of the correlation, and dot size indicates statistical significance. $^{*}p < 0.05$, $^{**}p < 0.01$ and $^{***}p < 0.001$. The red boxes in subgraphs D, E, and F were used to highlight the significant correlations between macrophages/neutrophils and the expression levels of TGM2, JAK3, and CCL2. GSEA, gene set enrichment analysis.

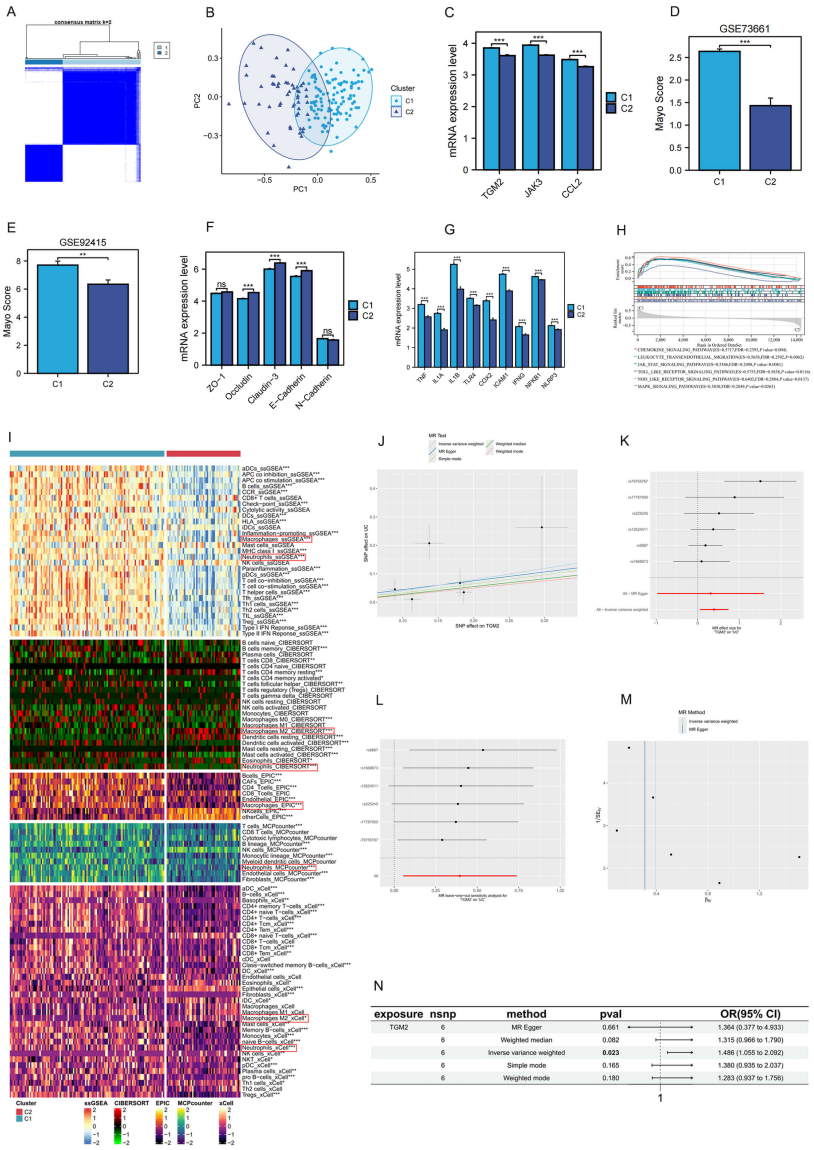

Fig. 5. Molecular subtypes of pediatric ulcerative colitis with distinct disease activity and genetic analysis of *TGM2*. (A) Pediatric UC samples were classified into two molecular clusters by consensus clustering based on the expression of *CCL2*, *JAK3*, and *TGM2*. (B) The distribution of Cluster 1 and Cluster 2 samples was evaluated by principal component analysis. (C) The expression levels of *CCL2*, *JAK3*, and *TGM2* were compared between the two clusters. (D) Mayo scores were compared between Cluster 1 and Cluster 2 in GSE73661. (E) Mayo scores were compared between the two clusters in GSE92415. Higher Mayo scores were observed in Cluster 1 in both cohorts. (F) The expression levels of ZO-1, Occludin, Claudin-3, E-cadherin, and N-cadherin were compared between the two clusters. (G) The expression levels of inflammation-related genes were compared between Cluster 1 and Cluster 2. (H) Differences in inflammation- and immune-related pathway enrichment between the two clusters were evaluated by gene set enrichment analysis. (I) Differences in estimated immune-cell abundance between the two clusters were assessed using ssGSEA, CIBERSORT, EPIC, MCP-counter, and xCell. The red boxes were used to highlight immune cell populations showing particularly pronounced differences in estimated abundance between the two clusters. (J) Associations of individual instrumental single-nucleotide polymorphisms (SNPs) with genetically predicted TGM2 expression and UC risk were assessed using five Mendelian randomization (MR) methods. (K) SNP-specific and combined MR estimates are presented as effect sizes with 95% confidence intervals. (L) The robustness of the inverse-variance weighted (IVW) estimate was evaluated by sequentially excluding each SNP in a leave-one-out analysis. (M) The distribution of SNP-specific estimates around the overall MR estimate is shown in the funnel plot. (N) Associations between genetically predicted TGM2 expression and UC risk were evaluated using MR-Egger, weighted median, IVW, simple mode, and weighted mode analyses. Statistical significance was obtained only with the IVW method. $^{*}p < 0.05$, $^{**}p < 0.01$, and $^{***}p < 0.001$; ns, not significant.

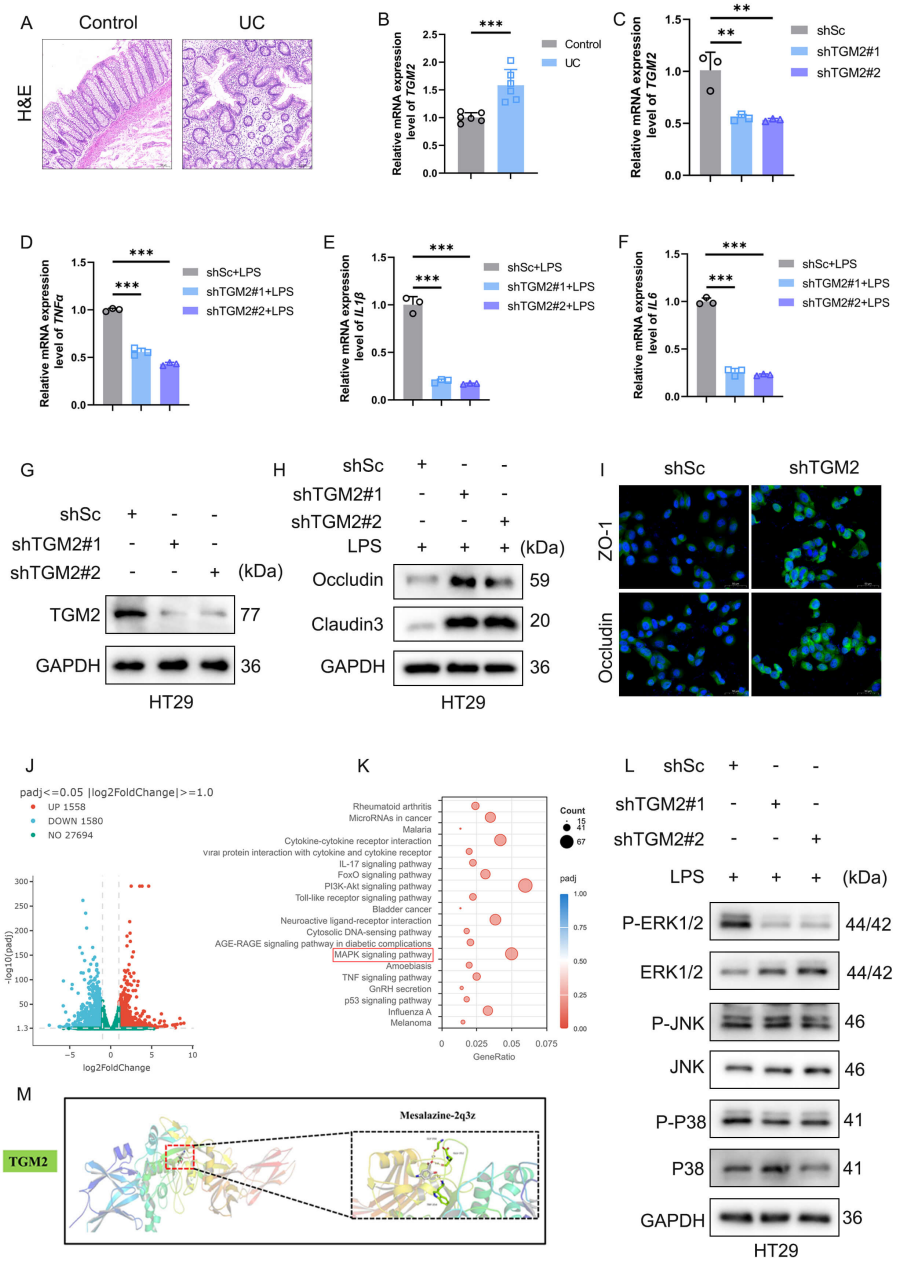

Fig. 6. Effects of TGM2 knockdown on inflammatory mediators, tight-junction proteins, and MAPK signaling in LPS-stimulated HT29 cells. (A) Representative hematoxylin and eosin staining of colonic tissues obtained from healthy controls and pediatric ulcerative colitis (UC) patients. Scale bar = 100 μm. (B) *TGM2* mRNA expression was measured in pediatric UC and control tissues. (C) TGM2 knockdown efficiency was evaluated at the mRNA level in HT29 cells transduced with two independent TGM2-targeting shRNAs. (D) *TNFα* expression was measured in LPS-stimulated shSc and TGM2-knockdown HT29 cells. (E) *IL1β* expression was measured in the indicated groups. (F) *IL6* expression was measured following TGM2 knockdown and LPS stimulation. (G) TGM2 knockdown was confirmed at the protein level by Western blotting. (H) Occludin and Claudin-3 protein levels were examined by Western blotting after TGM2 knockdown. (I) ZO-1 and Occludin expression was assessed by immunofluorescence staining. Scale bar = 50 μm. (J) Differentially expressed genes between LPS-stimulated shSc and shTGM2 HT29 cells are shown in the volcano plot. Using $|\log_2$ fold change$| \geq 1.0$ and adjusted $p \leq 0.05$ as the thresholds, 1558 genes were upregulated and 1580 genes were downregulated following TGM2 knockdown. (K) Kyoto Encyclopedia of Genes and Genomes enrichment analysis of the differentially expressed genes, in which the MAPK signaling pathway was identified among the enriched pathways. (L) ERK, JNK, and p38 phosphorylation were examined by Western blotting. Reduced ERK phosphorylation was observed following TGM2 knockdown, whereas no substantial changes in JNK or p38 phosphorylation were detected. (M) Predicted binding pose and amino acid interactions between mesalazine and TGM2 obtained by molecular docking. $^{**}p < 0.01$, and $^{***}p < 0.001$; ns, not significant.

95% CI 1.055–2.092; p = 0.023). The point estimates from the other methods were directionally similar but were not statistically significant: MR-Egger, OR 1.364 (95% CI 0.377–4.933; p = 0.661); weighted median, OR 1.315 (95% CI 0.966–1.790; p = 0.082); simple mode, OR 1.380 (95% CI 0.935–2.037; p = 0.165); and weighted mode, OR 1.283 (95% CI 0.937–1.756; p = 0.180) (Fig. 5J,K,N).

Sequential removal of individual SNPs did not materially change the IVW estimate in the leave-one-out analysis (Fig. 5L), and the funnel plot is shown in Fig. 5M. Nevertheless, the small instrument set, the lack of statistical significance with four complementary estimators, and the absence of colocalization analysis limit causal interpretation. The MR result was therefore regarded as suggestive genetic evidence rather than definitive evidence that TGM2 causes UC.

3.5 TGM2 Knockdown Is Associated With Reduced Inflammatory Responses, Increased Tight-Junction Protein Expression, and Lower ERK Phosphorylation

Colonic specimens from six pediatric patients with UC and six controls were included in the clinical validation (Fig. 6A), and *TGM2* mRNA expression was higher in the UC specimens (Fig. 6B). The raw PCR data corresponding to Fig. 6B are provided in **Supplementary Table 3**. Stable TGM2 knockdown in HT29 cells was confirmed at the mRNA and protein levels (Fig. 6C,G). After 24 h of LPS stimulation, TGM2-knockdown cells showed lower *TNF-α*, *IL-1β*, and *IL-6* expression and increased Occludin, ZO-1, and Claudin-3 abundance (Fig. 6D–F,H,I). The raw PCR data for Fig. 6C–F are provided in **Supplementary Table 4**. RNA sequencing of LPS-stimulated shSc and shTGM2 cells identified 1558 upregulated and 1580 downregulated genes after TGM2 knockdown (Fig. 6J), and the differentially expressed genes were enriched in the MAPK signaling pathway (Fig. 6K). The raw RNA-Seq data are presented in **Supplementary Table 5**. TGM2 knockdown was accompanied by reduced ERK phosphorylation, whereas substantial changes in JNK or p38 phosphorylation were not detected (Fig. 6L). These results suggest that, under the experimental conditions used in this study, changes in TGM2 expression were significantly associated with ERK pathway activation and tight-junction protein abundance. Molecular docking predicted a potentially feasible binding pose and hydrogen-bond interactions between mesalazine and TGM2 (Fig. 6M). Because this in silico analysis cannot demonstrate genuine physical binding, intracellular target engagement, or TGM2-dependent drug activity, the docking result was regarded only as preliminary evidence for generating a research hypothesis concerning a possible relationship between mesalazine and TGM2.

4. Discussion

The global incidence of pediatric UC has increased steadily over recent decades, with the most pronounced rise observed among children and adolescents [25]. Compared with adult-onset UC, pediatric UC is often characterised by more extensive disease involvement and a more aggressive clinical course, underscoring the importance of early diagnosis and effective intervention to achieve sustained remission and prevent long-term complications. At present, anti–tumour necrosis factor therapy remains the only biologic treatment formally approved for pediatric UC, highlighting a substantial unmet need for additional therapeutic strategies [26]. Although other biologics, such as vedolizumab and golimumab, have shown promise, significant gaps remain in the understanding of pediatric UC pathogenesis, disease monitoring, and treatment individualisation, as well as in addressing the unique developmental and psychosocial challenges faced by affected children and adolescents [27,28,29].

In the present study, an integrative analytical framework was employed to systematically examine the potential involvement of PANoptosis-related genes in pediatric ulcerative colitis. Seventeen genes were identified as differentially expressed between pediatric UC and control samples, with the majority showing increased expression in the disease group. Functional enrichment analysis indicated that these genes were mainly associated with inflammation-related pathways, including IL-4, IL-13, and IL-1 signaling. Following the integration of multiple machine-learning algorithms, CCL2, JAK3, and TGM2 were further prioritized as key candidate genes associated with pediatric UC [30]. Notably, *CCL2*, *JAK3*, and *TGM2* were consistently upregulated in both intestinal tissue and peripheral blood samples, and their expression levels were positively associated with disease severity, as reflected by the Mayo score. These findings support their potential value as biomarkers for assessing disease activity and progression. Treatment-associated changes in the expression of these genes were also observed following infliximab, vedolizumab, and golimumab therapy, with lower expression detected in treatment responders. Such findings suggest that variation in *CCL2*, *JAK3*, and *TGM2* expression may be associated with therapeutic response, although direct pharmacological regulation cannot be inferred. In addition, higher expression of these genes was associated with increased estimated infiltration of pro-inflammatory immune-cell populations, particularly M1 macrophages, neutrophils, and Th1 cells, which may collectively contribute to the establishment of an inflammatory intestinal microenvironment. Conversely, elevated expression was associated with reduced levels of barrier-protective molecules, including Claudin-3 and Occludin, further supporting a close relationship between inflammatory activation and epithelial barrier disruption in pediatric UC.

Previous studies have reported elevated TGM2 expression in UC and have linked TGM2 to mitochondrial dysfunction, altered cellular metabolism, and exacerbation of mucosal inflammation [31]. However, the pre-

cise mechanisms by which TGM2 contributes to UC progression, particularly in the context of inflammatory cell death pathways, have remained incompletely understood. In this study, Mendelian randomization analysis provided suggestive genetic evidence that increased TGM2 expression may be associated with a higher risk of UC. However, as Mendelian randomization alone cannot establish biological causality, TGM2 should be regarded as a potential contributor to UC pathogenesis rather than a confirmed causal driver. Moreover, molecular docking analysis predicted a potential binding pose between TGM2 and mesalazine, providing a basis for future studies to investigate whether TGM2 may be involved in the pharmacological effects of mesalazine in pediatric UC. Functional experiments showed that TGM2 knockdown in LPS-stimulated HT29 cells was accompanied by reduced expression of pro-inflammatory cytokines and increased abundance of the tight-junction proteins ZO-1, Occludin, and Claudin-3. However, these changes should not be interpreted as direct evidence of restored epithelial barrier function because functional permeability assays were not performed. Reduced ERK phosphorylation was also observed after TGM2 knockdown, whereas substantial changes in JNK or p38 phosphorylation were not detected. These findings suggest an association between TGM2 expression and ERK signaling under the present experimental conditions, but direct activation of ERK by TGM2 and ERK-dependent regulation of barrier function remain unproven. Moreover, the LPS-stimulated HT29 model reproduces only selected epithelial inflammatory responses and cannot fully recapitulate the cellular heterogeneity, immune–epithelial interactions, microbial influences, or chronic course of pediatric ulcerative colitis. Further validation using gain-of-function and rescue experiments, ERK modulation, functional permeability assays, patient-derived organoids, and *in vivo* colitis models is therefore required.

5. Limitations

Clinical validation was based on colonic samples from six pediatric patients with ulcerative colitis and six controls at a single center, and the observed difference in TGM2 expression should therefore be confirmed in larger, multicenter cohorts. *In vitro* experiments were conducted only in LPS-stimulated HT29 cells, which cannot fully reproduce the cellular heterogeneity, immune–epithelial interactions, microbial influences, or chronic course of pediatric ulcerative colitis. Further validation in additional epithelial models, patient-derived organoids, and *in vivo* models is required.

TGM2 was identified through PANoptosis-related bioinformatic screening, but canonical markers of pyroptosis, apoptosis, and necroptosis, together with direct cell-death assays, were not examined. Accordingly, TGM2 should be regarded as a PANoptosis-related candidate rather than an established regulator. Although TGM2 knockdown was associated with reduced ERK phosphorylation and increased tight-junction protein expression, gain-of-function, rescue, ERK-modulation, and permeability assays were not performed. The genetic evidence was also limited by the inclusion of only six SNPs, significance restricted to the IVW method, and the absence of colocalization analysis. In addition, molecular docking alone cannot confirm direct binding between mesalazine and TGM2, and further binding and TGM2-dependence experiments are required.

6. Conclusion

TGM2 was identified as a PANoptosis-related candidate associated with pediatric UC severity, inflammatory activity, tight-junction protein expression, and ERK phosphorylation. TGM2 knockdown was accompanied by reduced inflammatory-gene expression and increased ZO-1, Occludin, and Claudin-3 abundance in LPS-stimulated HT29 cells. The genetic analysis provided suggestive, but not definitive, evidence linking TGM2 expression to UC risk. These findings support further evaluation of TGM2 as a candidate biomarker and mechanistic research target; they do not establish TGM2 as a central regulator of PANoptosis, a direct activator of ERK, or a direct target of current UC therapies.

Availability of Data and Materials

The public datasets analyzed in the present study are available from the Gene Expression Omnibus database. This study used GEO database (https://www.ncbi.nlm.nih.gov/geo/), Metascape database (https://metascape.org/gp/index.html#/main/step1), GeneMANIA database (http://genemania.org/), Protein Data Bank (PDB) (https://www.rcsb.org/), GWAS summary data (https://gwas.mrcieu.ac.uk/), and the FinnGen database (https://www.finngen.fi/en/access_results). Additional data generated or analyzed during the current study are available from the corresponding author upon reasonable request.

Author Contributions

UC data were downloaded, processed, and analyzed by HD, LFD. Experiments were carried out by HD, LFD. HD and LFD wrote the draft. XJL is responsible for conception and supervision, and YFX participated in data interpretation and manuscript editing. The paper was revised by YFX, XJL. All authors read and approved the final manuscript. All authors contributed to editorial changes in the manuscript. All authors have participated sufficiently in the work and agreed to be accountable for all aspects of the work.

Ethics Approval and Consent to Participate

The study involving human participants was reviewed and approved by the Ethics Committee of Huaibei People's Hospital (No. 2023-109). Written informed consent was

obtained from all participants or their legal guardians prior to sample collection. All procedures were conducted in accordance with the Declaration of Helsinki.

Acknowledgment

Not applicable.

Funding

This research received no external funding.

Conflicts of Interest

The authors declare no conflicts of interest.

Supplementary Material

Supplementary material associated with this article can be found, in the online version, at https://doi.org/10.31083/FBL55382.

References

[1] Ordás I, Eckmann L, Talamini M, Baumgart DC, Sandborn WJ. Ulcerative colitis. Lancet (London, England). 2012; 380: 1606–1619. https://doi.org/10.1016/S0140-6736(12)60150-0

[2] Bouhuys M, Lexmond WS, van Rheenen PF. Pediatric Inflammatory Bowel Disease. Pediatrics. 2023; 151: e2022058037. https://doi.org/10.1542/peds.2022-058037

[3] da Silva BC, Lyra AC, Rocha R, Santana GO. Epidemiology, demographic characteristics and prognostic predictors of ulcerative colitis. World Journal of Gastroenterology. 2014; 20: 9458–9467. https://doi.org/10.3748/wjg.v20.i28.9458

[4] Ashton JJ, Beattie RM. Inflammatory bowel disease: recent developments. Archives of Disease in Childhood. 2024; 109: 370–376. https://doi.org/10.1136/archdischild-2023-325668

[5] Kobayashi T, Siegmund B, Le Berre C, Wei SC, Ferrante M, Shen B, et al. Ulcerative colitis. Nature Reviews. Disease Primers. 2020; 6: 74. https://doi.org/10.1038/s41572-020-0205-x

[6] Eisenstein M. Ulcerative colitis: towards remission. Nature. 2018; 563: S33. https://doi.org/10.1038/d41586-018-07276-2

[7] Ruemmele FM, Turner D. Differences in the management of pediatric and adult onset ulcerative colitis–lessons from the joint ECCO and ESPGHAN consensus guidelines for the management of pediatric ulcerative colitis. Journal of Crohn's & Colitis. 2014; 8: 1–4. https://doi.org/10.1016/j.crohns.2013.10.006

[8] McCoubrey LE, Seegobin N, Sangfuang N, Moens F, Duyvejonck H, Declerck E, et al. The colon targeting efficacies of mesalazine medications and their impacts on the gut microbiome. Journal of Controlled Release : Official Journal of the Controlled Release Society. 2024; 369: 630–641. https://doi.org/10.1016/j.jconrel.2024.04.016

[9] Kucharzik T, Koletzko S, Kannengiesser K, Dignass A. Ulcerative Colitis-Diagnostic and Therapeutic Algorithms. Deutsches Arzteblatt International. 2020; 117: 564–574. https://doi.org/10.3238/arztebl.2020.0564

[10] Kakiuchi T, Yoshiura M. Vedolizumab as the First-Line of Biologicals for Pediatric Patients With Ulcerative Colitis. Clinical Therapeutics. 2022; 44: 1028–1032. https://doi.org/10.1016/j.clinthera.2022.06.004

[11] Penagini F, Cococcioni L, Pozzi E, Dilillo D, Rendo G, Mantegazza C, et al. Biological therapy in pediatric age. Pharmacological Research. 2020; 161: 105120. https://doi.org/10.1016/j.phrs.2020.105120

[12] Sun X, Yang Y, Meng X, Li J, Liu X, Liu H. PANoptosis: Mechanisms, biology, and role in disease. Immunological Reviews. 2024; 321: 246–262. https://doi.org/10.1111/imr.13279

[13] Pandian N, Kanneganti TD. PANoptosis: A Unique Innate Immune Inflammatory Cell Death Modality. Journal of Immunology (Baltimore, Md. : 1950). 2022; 209: 1625–1633. https://doi.org/10.4049/jimmunol.2200508

[14] Pandeya A, Kanneganti TD. Therapeutic potential of PANoptosis: innate sensors, inflammasomes, and RIPKs in PANoptosomes. Trends in Molecular Medicine. 2024; 30: 74–88. https://doi.org/10.1016/j.molmed.2023.10.001

[15] Liu K, Wang M, Li D, Duc Duong NT, Liu Y, Ma J, et al. PANoptosis in autoimmune diseases interplay between apoptosis, necrosis, and pyroptosis. Frontiers in Immunology. 2024; 15: 1502855. https://doi.org/10.3389/fimmu.2024.1502855

[16] Koerner L, Wachsmuth L, Kumari S, Schwarzer R, Wagner T, Jiao H, et al. ZBP1 causes inflammation by inducing RIPK3-mediated necroptosis and RIPK1 kinase activity-independent apoptosis. Cell Death and Differentiation. 2024; 31: 938–953. https://doi.org/10.1038/s41418-024-01321-6

[17] Banoth B, Tuladhar S, Karki R, Sharma BR, Briard B, Kesavardhana S, et al. ZBP1 promotes fungi-induced inflammasome activation and pyroptosis, apoptosis, and necroptosis (PANoptosis). The Journal of Biological Chemistry. 2020; 295: 18276–18283. https://doi.org/10.1074/jbc.RA120.015924

[18] Franz M, Rodriguez H, Lopes C, Zuberi K, Montojo J, Bader GD, et al. GeneMANIA update 2018. Nucleic Acids Research. 2018; 46: W60–W64. https://doi.org/10.1093/nar/gky311

[19] Zhou Y, Zhou B, Pache L, Chang M, Khodabakhshi AH, Tanaseichuk O, et al. Metascape provides a biologist-oriented resource for the analysis of systems-level datasets. Nature Communications. 2019; 10: 1523. https://doi.org/10.1038/s41467-019-09234-6

[20] Sandborn WJ, Sands BE, Vermeire S, Leung Y, Guo X, Modesto I, et al. Modified Mayo score *versus* Mayo score for evaluation of treatment efficacy in patients with ulcerative colitis: data from the tofacitinib OCTAVE program. Therapeutic Advances in Gastroenterology. 2022; 15: 17562848221136331. https://doi.org/10.1177/17562848221136331

[21] Chen B, Khodadoust MS, Liu CL, Newman AM, Alizadeh AA. Profiling Tumor Infiltrating Immune Cells with CIBERSORT. Methods in Molecular Biology (Clifton, N.J.). 2018; 1711: 243–259. https://doi.org/10.1007/978-1-4939-7493-1_12

[22] Aran D, Hu Z, Butte AJ. xCell: digitally portraying the tissue cellular heterogeneity landscape. Genome Biology. 2017; 18: 220. https://doi.org/10.1186/s13059-017-1349-1

[23] Racle J, Gfeller D. EPIC: A Tool to Estimate the Proportions of Different Cell Types from Bulk Gene Expression Data. Methods in Molecular Biology (Clifton, N.J.). 2020; 2120: 233–248. https://doi.org/10.1007/978-1-0716-0327-7_17

[24] Dehghan A. Genome-Wide Association Studies. Methods in Molecular Biology (Clifton, N.J.). 2018; 1793: 37–49. https://doi.org/10.1007/978-1-4939-7868-7_4

[25] Kuenzig ME, Fung SG, Marderfeld L, Mak JWY, Kaplan GG, Ng SC, et al. Twenty-first Century Trends in the Global Epidemiology of Pediatric-Onset Inflammatory Bowel Disease: Systematic Review. Gastroenterology. 2022; 162: 1147–1159.e4. https://doi.org/10.1053/j.gastro.2021.12.282

[26] Vuijk SA, Camman AE, de Ridder L. Considerations in Paediatric and Adolescent Inflammatory Bowel Disease. Journal of Crohn's & Colitis. 2024; 18: ii31–ii45. https://doi.org/10.1093/ecco-jcc/jjae087

[27] Yokoyama K, Yamamoto Y, Nambu R, Hagiwara SI, Abukawa D, Mizuochi T, et al. Safety and efficacy of vedolizumab in pediatric patients with ulcerative colitis: multicenter study in Japan. Journal of Gastroenterology and Hepatology. 2023; 38: 1107–1115. https://doi.org/10.1111/jgh.16246

[28] Tokita K, Shimizu H, Takeuchi I, Shimizu T, Arai K. Long-Term Efficacy and Safety of Golimumab for Ulcerative Colitis in a Pediatric Inflammatory Bowel Disease Center in Japan. Pediatric Gastroenterology, Hepatology & Nutrition. 2022; 25: 461–472. https://doi.org/10.5223/pghn.2022.25.6.461

[29] Mansuri I, Wang S, Rufo PA, Liu E, Chan C, Bousvaros A. Efficacy and Safety of Sulfasalazine Suspension in Children With Ulcerative Colitis. Journal of Pediatric Gastroenterology and Nutrition. 2023; 76: 460–467. https://doi.org/10.1097/MPG.0000000000003698

[30] Greener JG, Kandathil SM, Moffat L, Jones DT. A guide to machine learning for biologists. Nature Reviews. Molecular Cell Biology. 2022; 23: 40–55. https://doi.org/10.1038/s41580-021-00407-0

[31] Wei W, Lu Y, Zhang M, Guo J, Zhang H. Identifying polyamine related biomarkers in diagnosis and treatment of ulcerative colitis by integrating bulk and single-cell sequencing data. Scientific Reports. 2024; 14: 18094. https://doi.org/10.1038/s41598-024-69322-6